Final Technical Report of NIAC Phase 1 Study

March 09, 2016

NASA Grant and Cooperative Agreement Number:
NNH-15ZOA001N-15NIAC (Proposal #15-NIAC-15A0134)

NIAC Phase I Study Period: June 2015 to March 2016

Thirsty Walls: A New Paradigm for Air Revitalization in Life Support

PI: Dr. John Graf

Environmental Control and Life Support Systems Branch

NASA Johnson Space Center

Houston, TX 77058

Email: john.c.graf@nasa.gov

Co-I: Dr. Mark Weislogel, Profesor

Department of Mechanical & Materials Engineering

Portland State University

Portland, OR 97201

Email: weisloge@pdx.edu

Co-I: Dr. Joan Brenecke, Keating-Crawford Chair Professor

Department of Chemical and Bimolecular Engineering

University of Notre Dame

Notre Dame, IN 46556

Email: jfb@nd.edu

Phase I Project Summary

This Phase I project Summary will be formatted as a series of summary statements, with additional comments. The summary statements are intended to focus on the most significant findings and discoveries – things that the project team knows now, but we didn't know at the beginning of the project.

1) **Direct Contact Between Gases is an ECLS System enabling capability.**

The Phase 1 project focused on CO2 capture, using direct contact of gases and liquids to facilitate the kinetics of solubility based absorption. At the beginning of the project, we were thinking about the CO2 capture application, but we were not thinking about ECLS system level impacts. In the course of the phase 1 effort, we realized that many fundamental unit processes in biological and chemical systems (absorption, evaporation, transpiration, distillation, condensation) need direct contact between a gas phase system and a liquid phase system. Capillary technology that enables gas absorption into a liquid helps all ECLS processes that involve gas absorption – it also enables evaporation, transpiration, distillation, and condensation. Fluid management capability is more broadly applicable than we had originally thought.

2) **CO2 capture using liquid sorbents in microgravity is feasible.**

The phase I project set out to assess feasibility of the CO2 capture application. Liquid pumping rates are sufficient, high viscosity is tolerable, contact area is sufficient, flow distribution networks are initially large, but there are design paths to reduce system size. It is feasible to use direct gas/liquid contact for CO2 capture, and with the right designs and sufficient development, these systems promise to be smaller, more power efficient, and more reliable that current systems.

3) **There are other ways to contact gases and liquids – but thin film capillary techniques are new, exciting, and have amazing potential.**

As a result of this phase I project, we are able to put thin film contactors in context with other fluid management systems. Once placed in context, the power and significance of thin film contact becomes apparent. Two existing methods of gas/fluid management are membrane contactors, and wet spray reactors. Membrane contactors have nearly perfect liquid containment, but unacceptably slow kinetics. Wet spray contactors have great kinetics, but no gas/liquid containment. In the balance between kinetics and containment, thin film contactors are in the "goldilocks zone" – they have sufficient kinetics and sufficient control. This is new and potentially powerful.

4) **ECLS system reliability is the key to exploration missions – the key to reliability is having system attributes that favor reliability**

Slow moving, gently sweeping, uniform rate, ambient temperature, ambient pressure systems are more likely operate reliability than systems that involve vacuum systems, high temperatures, hazardous chemicals, and transient operating conditions. If mission planners place a priority on system reliability, ECLS system developers should focus on processes that have the attributes of reliability.

5) **The processes with favorable reliability attributes tend to be biological.**

Biological systems tend to be ambient temperature, ambient pressure, free of hazardous chemicals, operate at a steady rate, and have the attributes of reliable systems. If Mission Planners want a reliable ECLS systems, then ECLS system developers should increase the technical maturity of biological systems. Biological wastewater processes can credibly achieve >98% recovery of water from wastewater. Biological algae based systems can credibly achieve >75% oxygen from CO2.

6) **The single greatest impact on launch mass of an ECLS system is water. The best way to enable biological water processing is to develop a capillary based method of urine capture that doesn't use pretreat chemicals.**

The ISS potty uses a rotary phase separator that needs strong pretreat chemicals to prevent biofouling and clogging caused by precipitate build up. These pre-treat chemicals, by design, are intended to kill all microorganisms. Rotary phase separators and biological wastewater systems are essentially incompatible. The most enabling thing a fluid mechanics expert can to is to capture urine without the use of pretreat chemicals. This is one of the central technical tasks of the Phase II proposal, the project team has already developed and patented capillary methods of capturing urine in a potty environment. Forward work would involve testing the long term effectiveness of frequent rinsing and occasional system dry out, heat sterilization.

7) **There is good, promising, forward design and development work – but no fundamental "show stoppers" – to develop a thin film liquid sorbent CO2 capture system.**

Thin film fluid management starts with several constraints – everything in contact with the air is at the same pressure, and fluids generally move because of a pressure gradient. Thin film fluid flow must rely on capillary gradient, with is a slow and relatively feeble process. The practical limits of fluid movement is just a few centimeters. Phase I identified that a CO2 capture system needs a traditional closed pipe pumping system to deliver liquids through thousands of ports across a broad area in order to have sufficient contact area. Phase I fluid sizing calculations (shown in detail in this report) show that the pumping and manifold system will likely be bigger and weigh more than the capillary surface. Phase I efforts also show that there are lots of design ideas to make this new system smaller and more effective. It is feasible to make a thin film system.

8) **The most capable Ionic Liquids are not presently feasible, but other chemically active liquids can be used to make an effective thin film CO2 capture device.**

Dr. Brennecke and the Notre Dame group were key members of the Phase I team, and they are not on the Phase II proposal team. They did nothing wrong, this group is awesome. Two of Dr. Brennecke's students developed candidate ILs with properties that best matched NASA's needs. The candidate IL had amazing capacity (41% by weight) and low regeneration temperatures (significant cyclic performance with regeneration temperatures as low as 60C). But the IL was not stable, after a few tests it produced a strong odor – indicating chemical breakdown. This has several implications: The first is that Phase I feasibility study results indicate that IL based systems with 40% cyclic capacity are not likely. But that doesn't mean that CO2 capture using liquids isn't feasible. There are other ionic liquids and commercially available amines that have good stability, low vapor pressure, and capacity in the 10-15% range. These kinds of systems would represent significant improvements, but not transformative ones. The Brennecke group's top priority is doing fundamental development work on ILs. NASA needs fundamental development work to occur, but not as part of a NIAC feasibility study. Dr. David Klaus at

CU has an NSTRF sponsored doctoral student who is studying ILs for NASA ECLS applications. Jordan Holquist is relatively less interested in doing fundamental chemical development and relatively more interested in considering the use of ILs for NASA ECLS applications. Dr. Klaus and Jordan Holquist will lead IL efforts in the NIAC Phase II proposal, because they are a better fit. But look for future proposals with collaborations between JSC, University of Colorado, and Notre Dame in the area of technology development of ionic liquids. Anything with the potential of achieving 40% capacity and regeneration temperatures below the boiling point of water needs to be further developed.

9) The C9 reduced gravity flight showed feasibility – and taught us about flow instability issues.

The C9 reduced gravity aircraft test campaign was an incredible experience. The ability to see films develop, cavitation to occur, and systems recover from cavitation was monumentally helpful. But the real benefit of the test campaign was to gain a deeper understanding and appreciation of fluid management – especially fluid management with multiple pumps. There is a difference between knowing the data and having an understanding. C9 results are shown in greater detail later in the report.

10) Capillary fluid management has ECLS system wide implications.

We started the Phase I effort thinking about test articles and CO2 capture subsystems. We finished the Phase I effort thinking about a system level ECLS design with thermal management, air revitalization, and water recovery systems. It is exciting to think about things at a system level, and it is invigorating to plan collaborations with researchers that I've never collaborated with before.

Table of Contents

1.0 C-9 Reduced Gravity Flight Experiment

1.1 Introduction

The use of liquid systems in space is challenging due to controlling and balancing fluid flow, the complexity of gas/liquid contacting, and separation of gas and liquid phases. The development of additive manufacturing such as 3D printing has allowed for the creation of complex capillary structures, not previously attainable through traditional subtractive manufacturing techniques using mills, lathes, EDM, or similar. As an assembly, these capillary structures can be linked and formed into microchannel reactors, which allow for large surface area gas/liquid contact in microgravity and uniform fluid flow management. Additionally, these capillary structures capture and transport liquid using surface tension and capillary action, making them suitable for use with liquids in the absence of gravity.

The project development team explored microchannel reactors paired with liquids as a means to provide a more energy efficient and reliable method of removing humidity and CO2 from the air. In order to gauge viability of this technology in relevant spaceflight environments, the behavior and characteristics of the thin membrane generated in capillary structures were studied in microgravity.

1.2 Test Objectives

The test objectives for this activity were as follows:

1. Observe the effect of pumping rates on liquid film formation
2. Achieve uniform flow throughout the microchannel reactor
3. Balance flow rates in the system plumbing at the reactor inlet and outlet
4. Observe film development and thickness around the air/liquid contacting surface
5. Proof of concept – deployment of a liquid film via bifurcating channels to a contacting air/liquid surface in microgravity

1.3 Description of Test Conducted

NASA's C-9 reduced gravity aircraft follows an elliptic flight path consisting of 40 parabolas. When the aircraft undergoes elevation for each parabola at 45 degrees nose high and reaches a constant altitude, microgravity is achieved for the following 25 seconds before descending. For this experiment, liquid film thickness as function of fluid

properties and pumping velocity in a capillary driven microchannel reactor was observed for each 25 second zero-g interval. At the onset of each parabola, 500 ml of viscous liquid was sent to a dendritic microchannel reactor using a single peristaltic pump. The liquid continued to recirculate through the reactor in a closed-loop during reduced gravity. Three test parameters were altered every 10 parabolas – pumping rate, valve setting, and reactor tilt angle.

1.4 Description of System Configuration

An aluminum frame structure, with a main and secondary base plate, was used to house all system components (See Figure). The plates were separated using 2" aluminum channel supporting both the perimeter and the center of the plate for vibration isolation. On the main plate, accelerometers, valve controls, a pump setting controller, timer, and switch panel were installed. All remaining system components were mounted to the base plate. A peristaltic pump circulated viscous fluid through a recirculating closed-loop containing the dendritic reactor. A needle valve was placed at the reactor inlet and outlet for flow rate control. A purge loop was incorporated to release the buildup of entrained air.

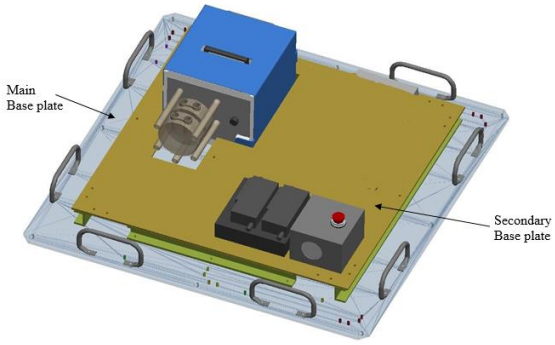

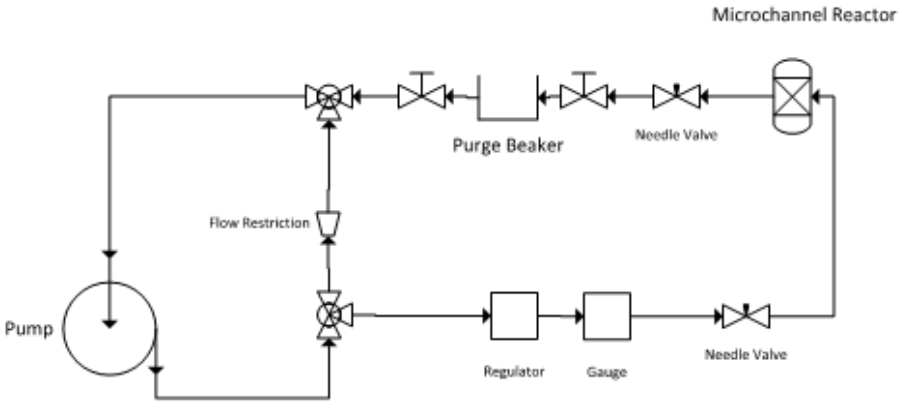

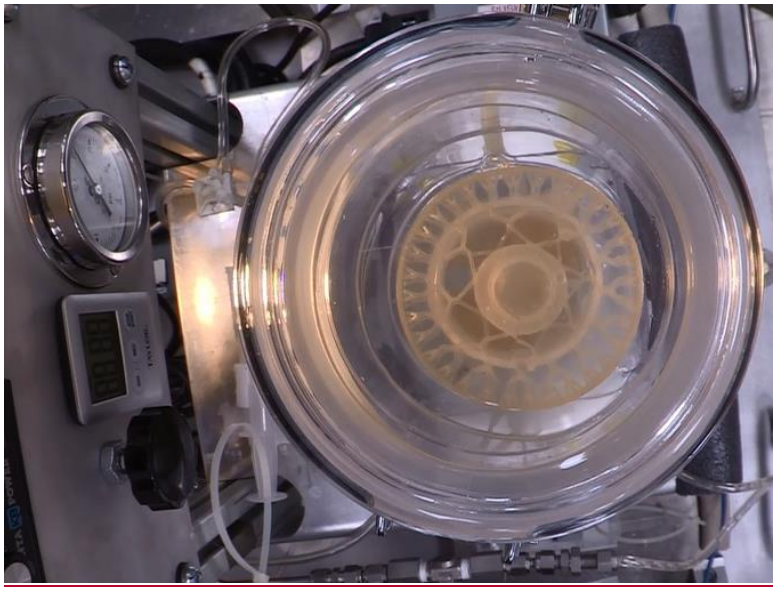

1.5 Conclusive Findings

Achieving uniform liquid flow throughout the reactor proved to be difficult. A balancing act between the inlet and outlet needle valves had to be manually performed each parabola.

Uniform flow and the desired reactor thin-film annular ring were not observed. When the inlet flow rate exceeded the outlet rate, the microchannel reactor would overflow, causing the annular film to thicken and protrude. When the outlet flow rate exceeded the inlet rate, a fully developed film around the reactor's air/liquid contacting surface did not form. Also, air was pulled in through the withdrawl ports, resulting in entrained air bubbles in the bifurcating channels and system plumbing. Air bubbles quickly accumulated and system operation had to be ceased in order to purge the lines. Although the film alternated between protruding and cavitation, the liquid maintained contact with the reactor in microgravity because of capillary forces and did not release into the surrounding atmosphere.

Film protruding:

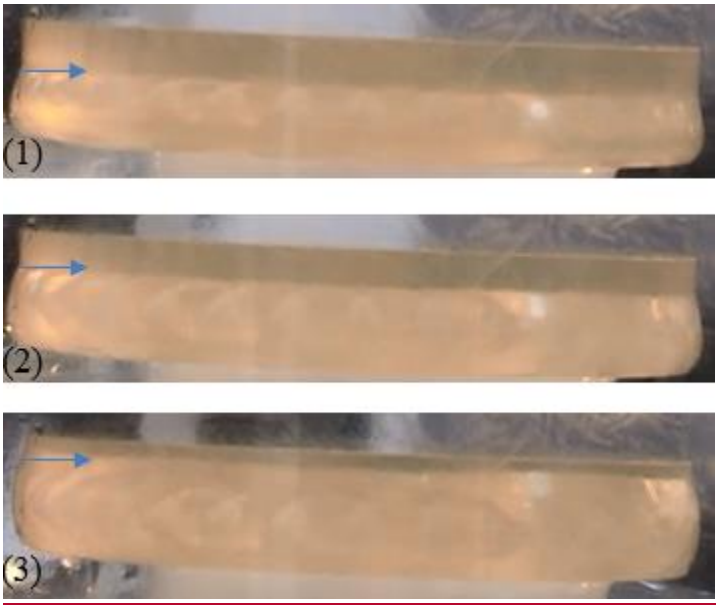

Film Cavitation:

Cavitation in dendritic channels:

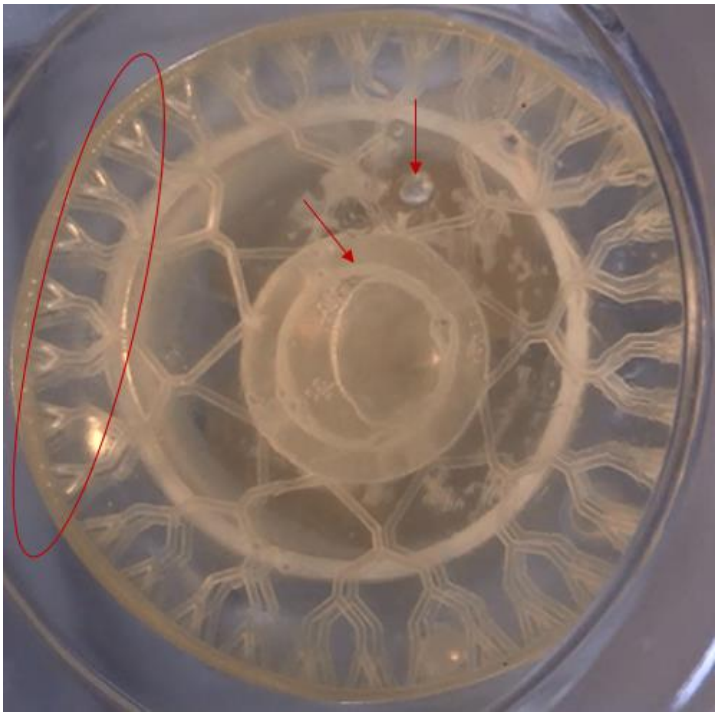

2.0 Study of Ionic Liquids

2.1 Introduction

ILs are salts with low melting points, wide liquid operating ranges, and endless tunability. They are attractive for spacecraft CO_2 capture and regeneration because they have immeasurably low vapor pressures, their interactions with CO_2 and selectivity over other gases can be tuned exquisitely, and no added water is needed (which reduces the volumetric capacity and adds an energy penalty during regeneration for alkanolamine-based CO_2 capture).

Over the last fifteen years, the IL research team at Notre Dame has made both fundamental scientific and technological advancements in the development of ILs for post-combustion flue gas separations. Our group was the first to report high physical CO_2 solubility in ILs.[1] Subsequently, we have led the world in modifying ILs for higher physical dissolution of CO_2 and high selectivity over O_2, N_2, H_2, CH_4, H_2S and other gases.[2-5] Since 2004, our funding from the DOE NETL and ARPAe programs has led us to focus exclusively on CO_2 separation from conventional coal-fired power plant post-combustion flue gas streams where the CO_2 partial pressure is ~ 0.15 bar. As a result, we quickly moved to incorporation of chemical complexation, based on amine functionality, in the ILs.

2.2 Justification for Study Approach

1. *Doubling the capacity.* Carbon capture using conventional aqueous amines is limited by the requirement that two equivalents of the amine are necessary for each molecule of CO_2 captured (eqs. 1 and 2). In contrast, based on discoveries made using theoretical calculations,[6,7] we showed experimentally that a 1:1 reaction stoichiometry

is observed when the amine functionality is tethered to the anionic component of an IL, effectively doubling the molar capacity for CO_2.

2. *2. Eliminating viscosity increases*. Since the first report of an amine tethered to an IL,[11] dramatic increases in viscosity upon complexation with CO_2 have been observed.[8,10,12] This increase in viscosity is due to the formation of a salt bridge network.[13] However, we were able to eliminate this undesired side-effect by employing novel Aprotic Heterocyclic Anion (AHA) ILs to frustrate the formation of these hydrogen bonding networks.[9,14] Examples of effective AHA ILs include the phosphonium salts of pyrrolides and pyrazolides; viscosities before and after CO_2 complexation are comparable, as shown in the figure.

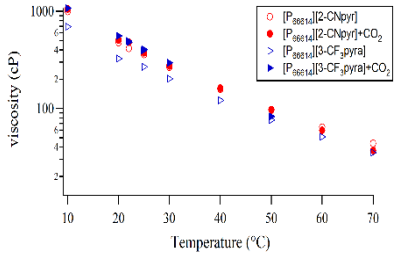

3. *3. Tuning reaction enthalpy*. By using various nitrogen based heterocycles along with appropriate electron withdrawing or donating groups, we have been able to design and synthesize AHA ILs with CO_2 reaction enthalpies ranging from –31 kJ/mol (relatively weak bonding) to –80 kJ/mol (strong bonding).[14]
4. IL's have a favorable capacity for CO2 (we captured 41% in 6 hours)

1.3 Description of Test Conducted

Characterization testing of saturation, loading, desorption

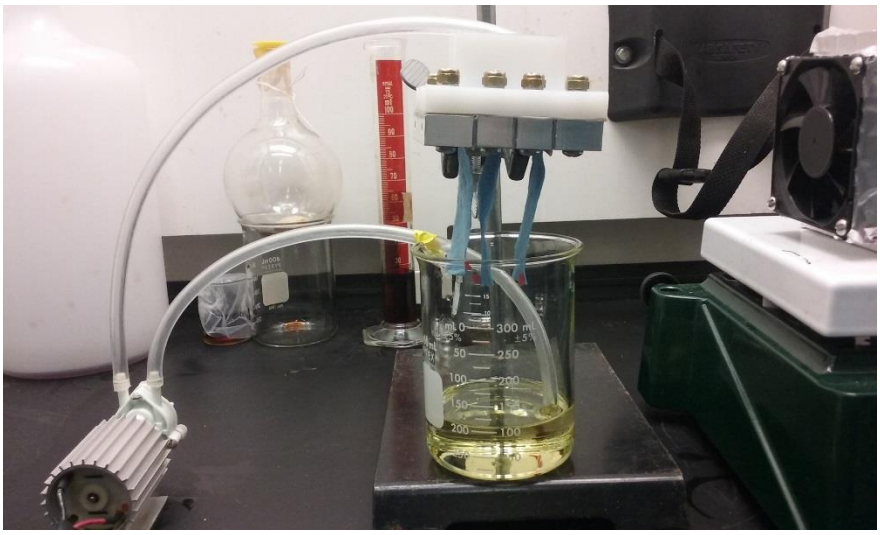

1.4 Summary of Lessons Learned

IL has favorable loading capacity (we got 41%)
However, IL received destabilized

3.0 CO2 to O2 Conversion Investigation

3.1 Background

3.2 Description of work Conducted

3.2.1 Trade-Study: Algae for Oxygen Recovery

Theoretical Recovery Calculation

Theoretical O_2 Recovery from CO_2 is 100%

Reviewing the equation for photosynthesis (Eq 1.) shows that theoretically 100% of O_2 should be recovered from CO_2.

$$6H_2O + 6CO_2 + \text{energy} \rightarrow C_6H_{12}O_6 + 6O_2 \qquad \text{(Eq.1)}$$

Due to mechanisms of O_2 transportation within the algae cell, the resulting O_2 recovery is closer to 95%. It should also be mentioned that for a given amount of CO_2 dissolved into the algal medium, ~85% of it is absorbed by the algae and used in the above equation. This is more than the current ISS recovery percentage of ~50% using the Air Revitalization System. It also surpasses the NASA Technology Roadmap requirement of 75% for extended spaceflights.

Algae in Various Temperature Environments

Algae can thrive in a wide range of temperatures

Studies have shown that algae are viable and reproduce in temperatures from 4°C up to 35-50°C, depending on the species and CO_2 concentration. Higher plants typically have a reduced range of temperatures from 5°C to 25°C or 10°C -35°C depending on the plant's preferred temperate zone. Algae's wide temperature range gives the cultivator the flexibility of managing CO_2 levels without regards to restrictive temperature bounds. [4,5,6]

Algae Air Revitalization vs Sabatier and Oxygen Generation Assembly

Air Revitalization through Algae is Safer than Sabatier and Oxygen Generation Assembly (OGA)

Unlike the algae photobioreactor, both the Sabatier and the OGA system consume and yield hazardous products. The Sabatier system requires hydrogen (H_2) gas to reduce CO_2 into methane (CH_4) and water (H_2O). While the produced water doesn't pose as many risks, hydrogen and methane are very flammable gasses, and could cause asphyxiation if leaked into the cabin. The Sabatier system utilizes an exothermic reaction with an operational temperature of ~430°C and produces a lot of heat. This could cause fires or melt components

if not disposed of properly. The OGA uses the water produced by the Sabatier system to electrolyze it into O_2 and H_2. Comparing both the Sabatier system, and the OGA to an algal photobioreactor showcases the safety that a photobioreactor can bring to air revitalization technologies.

Using thirsty walls to support an algal photobioreactor will consume less power than the current air revitalization technologies on the ISS. The algae photobioreactor would be able to replace the functionality of the Sabatier and the Oxygen Generation Assembly (OGA). The following Table 1 contains current ISS number, and the algae photobioreactor was scaled for a crew of 4. The algae numbers reflect just the lights needed to illuminate the medium

	Volume (m^3)	**Mass (kg)**	**Power (kW)**
Sabatier & OGA		613	4.0
Algae	1.04	1064	3.3

Other functions of algae include thermal control and radiation shielding. It is hypothesized that algal medium could be used in place of water in spacecraft cooling loops, but the viability of the algae during this operation has to be confirmed experimentally. Lining the inside of the spacecraft cabin with algal medium and biomass may provide radiation shielding, due to water's excellent shielding characteristics

3.2.2 Design of Algae System for Phase II

A capillary driven algae photobioreactor concept has been designed

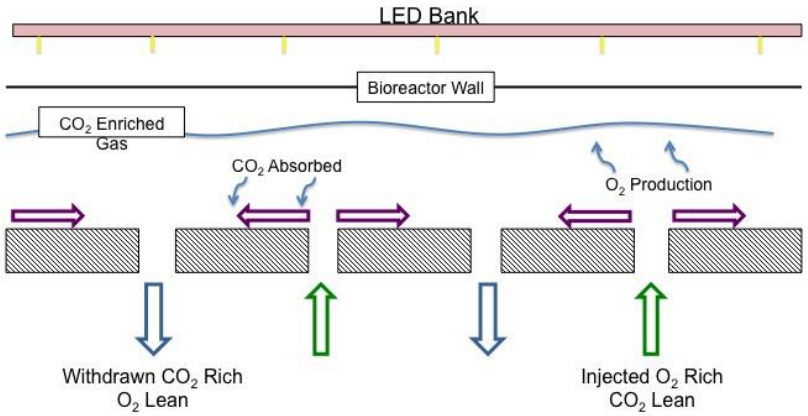

The algae medium uses the same method of transport as the IL through the capillary contactor. In order to attain high rates of oxygen recovery, concentrated CO_2 needs to be passed over the algal medium instead of cabin air. The bioreactor will be contained due to the high CO_2 concentration. As the concentrated CO_2 gas passes over the exposed medium, it will be absorbed by the medium via Henry's Law. As the algae recover the O_2, it will be released into the sweeping CO_2 stream using the transport based off of Henry's Law as well.

4.0 Water Processing Investigation

4.1 Current Technology

Current water recovery systems that employ only physical and chemical processes are intensive users of resources, and ultimately result in trading the cost of stored water for the costs of power consumption and consumables and require the use of large masses of hazardous chemicals for urine stabilization. Chemical urine stabilization is currently practiced in order to prevent biological activity in the urine collection system, particularly the urine air separator, and desalination unit. The current urine collection system and urine processor (rotary distillation) is sensitive to solids formation including biofilms (bacterial or fungal) and solid precipitates which occur as the pH rises due to urea hydrolysis. This pH rise would also cause substantial carry over of NH_3 through the urine processor to its product water. While chemical stabilization is currently able to prevent these issues, it requires the continuous use of highly hazardous fluids. It's use also results in a brine that is difficult to dewater and does not allow for recycling of carbon and N, as well as produces a hazardous solid waste that must be stored (Jackson et al., 2014). These issues will only increase for long duration missions out of low Earth orbit, particularly if the habitat includes hygiene or laundry components. Without frequent resupply and with the addition of other waste streams, the habitat would have to store large volumes of highly hazardous fluids and brine solids.

4.2 Biological Process Selection

Biological processing in micro-gravity requires specialized systems to allow O_2 delivery and removal of metabolic gasses without two phase flow. This has been successfully achieved by using Membrane Aerated Bioreactors (MABR). MARBs use semi-permeable membranes to concomitantly provide an attachment surface for biofilm immobilization and a conduit for diffusive oxygen transport, to provide the aerobic environment (Figure 1). MABR operation and efficiency is a combination of the type of membrane used (e.g. fiber vs sheet), membrane material (e.g. dense, microporous, composite), reactor configuration (e.g. specific surface area) and operational regime (e.g. gas/liquid pressure, degree of biofilm management). Very high rates of treatment can be achieved with active biofilm management which can include forced shedding using inert gas mixing or high liquid flow velocities with the utilization of extensive control systems, and the need for continuous treatment of the biosolids waste flow. MABRs can also be operated without

active biofilm control (Kubista et al., 2012). Using lower specific surface areas (~100-200 m^2/m^3) and longer hydraulic residence times, MABRs can operate with minimal biomass loss. This leads to long solids retention times with low reactor volumetric efficiency, but provides simple operation and limited need for solids management (Jackson et al., 2009).

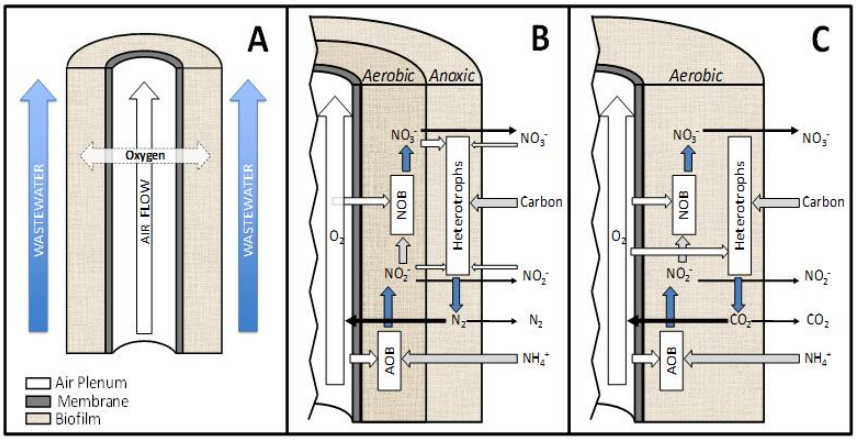

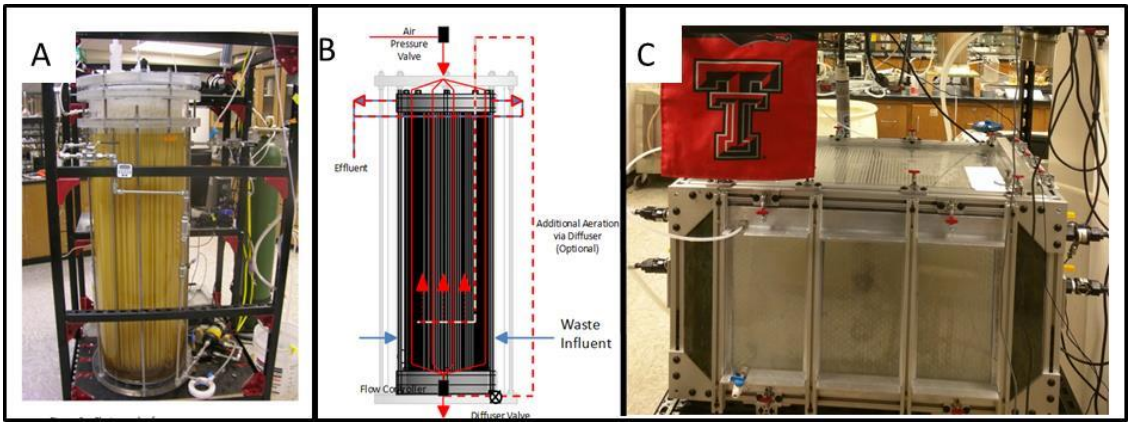

Biological treatment using a reactor such as CoMANDR is capable of treating habitation wastewater in microgravity. It currently relies on pressurized flow to move the wastewater across the membrane surface and pressurized air to allow advective flow through the membrane lumens, and is reasonable compact (0.2 m^3/crew of 4). It integrates well with the thirsty wall concept by controlling downstream biomass production on surfaces, producing flush water compatible with a static urine air separator, provides nutrients for the algal reactor and can process spent algal growth solution, and produces N_2 and CO_2 for reuse as make up air or carbon for the algal reactor.

It is also possible that the biological processor could be incorporated within the Thirsty Wall process. A bioreactor that was designed to use capillary forces to move thin films of wastewater across a gas permeable surface could allow increased treatment with a low volumetric foot print. It would also eliminate the need for pressurized operation, pumping liquids, and compressed gas flow. Its incorporation into the wall structure would allow much larger surface areas to be used leading to much more robust treatment and higher

treatment efficiencies while also providing additional shielding. Evaporation would also reduce the load on the desalination system by perhaps up to 50 to 75 %.

5.0 Gas/liquid Contacting and Fluid Management

The efficiency of species transport across fluid interfaces is dramatically enhanced for thin fluid films. Unfortunately, the viscous resistance of such films is high, requiring both high pressures and short distances to circulate such fluids in direct contact reactor applications. Nature accomplishes such feats in large lumbering processes through dendritic manifolds as suggested by the 'tree' analogue in Fig. 1a. The 'pump' draws fluid through the dendritic root structure through the trunk and through the leaves. Passive 'chemistry' is conducted on the fluid between the leaves and the roots. This same system is re-presented in Fig. 1b where the passive 'chemically active' liquid is directly convected through open channels exposed to a chemically active air stream. A number of capillary channel geometries are capable of performing this function and three are shown in Figs. 1c-e for single wedges, porous tubes, and corrugated sheets, respectively.

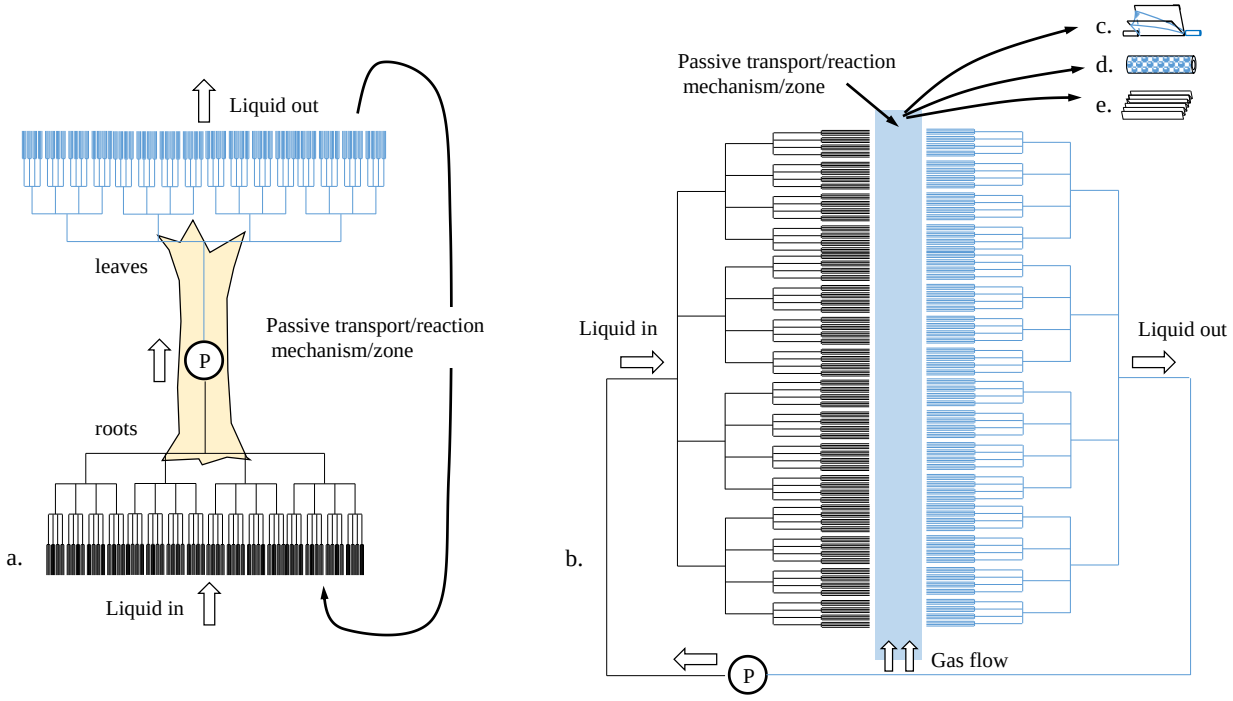

Fig. 1. a. Dendritic flow network in 'tree-form' analogy where the pumping for the system is represented by the trunk and the passive liquid return mechanism implied by the leaf-to-root transpiration-condensation mechanism. b. The same network in a. is reorder for the smart walls application in a low-g environments where a single pump both delivers to and returns liquid from a large parallel array of open capillary free surface contactors with a reacting air flow stream. A selection of demonstrated capillary conduits in shown in c. single wedges, d. graded porosity perforated tubes, and e. corrugated walls.

In the example systems in Fig 1a and 1b, it is clear that the manifolds necessary to direct the liquid to the 'reaction zone' are large in terms of volume and mass, and complex in terms of potential susceptibility to flow rate balancing, contamination, and damage. These concerns for engineered systems are mitigated by 3D printing complex shrouded and ducted networks to perform numerous passive functions with low pumping power requirements and minimized system volume and mass. A simplified schematic of a one configuration of the low-g capillary contactor is shown in Fig. 2. The perspective figure of Fig. 2a shows both manifold and narrow air flow passage for this low-g capillary wedge flow contactor (wedge conduits exaggerated for clarity). A planform image of the manifolds is shown in Fig. 2b. The 4-fold (fractal) nested manifold is shown in 2c along one leg of the device. A resistor model of the manifold-level legs of the device is shown in Fig. 2d, which may be solved explicitly to find the viscous flow resistance elements

$$\boldsymbol{R}_i = \frac{n}{1+i}\frac{(P_{in}-P_{out})}{Q_{in}} \tag{1}$$

and

$$R_i = \frac{n}{Q_{in}}\left[P_{in} - P_{out} - \sum_{j=1}^{i}\left(\frac{n-j+1}{n}\right)\boldsymbol{R}_j\right] = \left(\mathrm{C}\frac{\mu L}{r^4}\right)_{Ri}. \tag{2}$$

In eq. 2, *C* is the geometric resistance coefficient for the duct shape (circular, square, rectangular, etc.). The flow rate across each capillary wedge channel sketched in magnification in Fig. 3 is given by

$$Q_i = K(\alpha,\theta)\left(\frac{H^3}{L}\frac{\sigma}{\mu}\right)_i, \tag{3}$$

where $K \sim 0.01$, □ is the surface tension, and □ is the dynamic viscosity of the liquid. Eqs. 1-3 are readily balanced and employed to compute overall system performance metrics. For example, for the device sketched in Fig. 2a the total system volume is 0.2 m^3 (200 L). Allowing only a 0.7 psi pressure drop through the device, cascading manifold tube diameters are chosen such that 68% of the device volume (137 L) is liquid, 72% of which resides in the wedge channels and 28% in the manifold. Thus manifold reduction is not the primary means of reducing total liquid volume. (We note that a typical maple tree contains a minimum of 50 L of sap.) Reductions in liquid volume of up to 50% may be achieved by reducing capillary wedge channel depth *H* and increasing corner half-angle □. Further reductions may be achieved by accepting larger pressure drops. For example, a 4-fold reduction in manifold mass and liquid volume may be achieved by an approximately 10-fold increase in pressure loss. But again, for this design, manifold volumes are not the majority of the liquid content. Reducing film thickness is the primary means of reducing liquid inventory for a fixed surface area direct contactor and we note that a minimal 1mm thick film for a 10 m^2 device is already at 10 L. But such films are extremely slow moving for viscous Ionic Liquids (ILs).

The electrical resister analog approach of Fig. 2 is enabled by a laminar flow assumption for the presumed high viscosity ionic liquid. The circuit is solved explicitly for the first manifold pair for

upstream manifold resistance element $\boldsymbol{R}_i$ and downstream manifold resistance element R_j. These forms may be determined for every cascading manifold pair and thus every viscous resistance element in the device. Traditional pipe network fabrication of such a device is significantly complicated by numerous aspects of the design including a lack of continuously varying COTS duct diameters, but such devices are readily constructed via large scale 3-D print methods. The analytical approach allows all conduit dimensions, pressure drops, and flow rates to be determined as functions of contactor area, overall pressure drop, open wedge conduit dimensions, and temperature-dependent fluid properties (contact angle, viscosity, density, and surface tension).

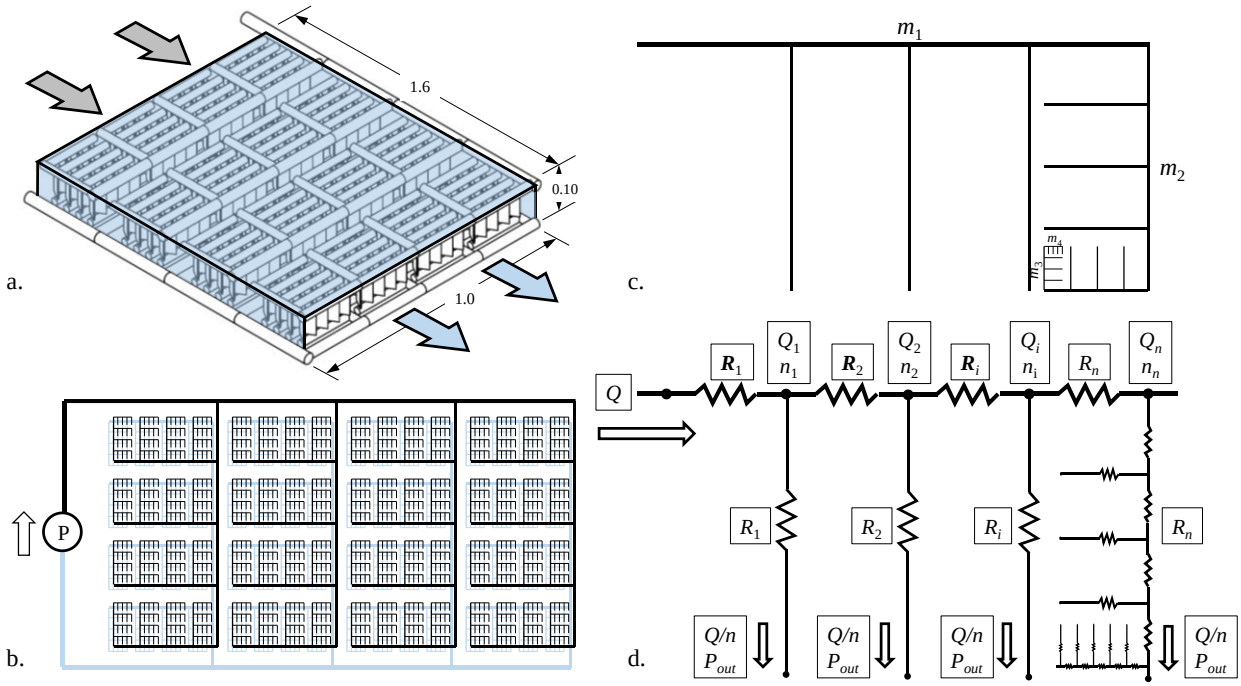

Fig. 2. a. Perspective view of practical configuration for Fig. 1b system for 10 m^2 surface area within a 1.6 by 1.0 by 0.1 m narrow duct architecture. Air flow indicated by arrows. A planform view of the network is shown in b. The fractal nature of the nested manifolds is shown in c. for a single 'leg' of the device. The resistor model for the 4-tier fractal leg of c. is shown in d. which may be balanced and solved explicitly.

The design process is demonstrated briefly here for a contactor with the following characteristics

- 10 m^2 interface/contactor area
- 10 cm long L_w = 2 cm, H_w = 2 cm high, 2□ = 30° open wedge conduits
- Ionic Liquid (IL): □ = 0.02 kg/m·s, □ = 1000 kg/m^3, □ = 0.05 N/m, □ = 50°

From only these requirements our model quickly determines the device sketched in Fig. 2a which meets the 10 m^2 area with the following characteristics:

- Device envelope: 1.6 m by 1.0 m by 0.12 m.
- Max. Liquid flow rate: 142 L/min
- Max. Pressure drop: 0.7 psi
- Max. System Liquid volume: 137L
- Max. Mass: 137 kg

- Manifold diameters are 4, 3.6, 2.8, and 2.6 cm
- Manifold volumes are: 0.004, 0.008, 0.008, and 0.017 m^3

These values are maximums. The flow rate may be reduced, which in turn reduces DP. Manifold dimensions may also be reduced according for low flow rates while still maintaining system DP.

Notional Nested Manifold Micro-Gravity Designs

Drawing from the nested manifold concept, various direct contactors are envisioned. The design approach of Fig. 2 is a rectangular slot Cartesian architecture exploiting single wedge capillary devices for the contactor. Two essentially axial designs are depicted in Figs. 3 and 4. Fig. 3 presents a solid model of a 4-tier manifold where corrugated walls consisting of capillary wedges are aligned radially, passively delivering liquid across the air gap from the inlets along the center axis to the outlets along the outer circumference. A section view is provided at lower right in Fig. 3 demonstrating that high packing densities are possible with such an approach with stable capillary controlled surfaces (films).

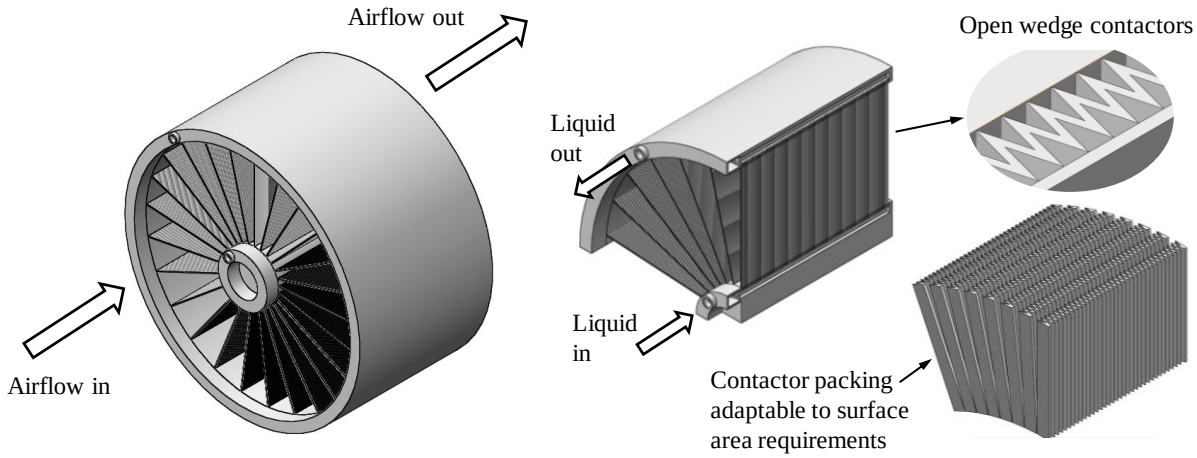

Fig. 3. Four-tier open wedge corrugated wall axial low-g contactor with sectional cutaway views illustrating manifold options and interior corner detail.

A stackable 4-tier open wedge corrugated wall axial low-g contactor with sectional cutaway and planform views and direct contact porous tubes is shown in Fig. 4. In this design, capillary forces are used to stabilize the interfaces along the porosity gradient of the tubes, which allows for increasingly stable interfaces despite the increasing pressure drop across the tube wall. Unlike the previous capillary driven wedge contactor systems, in this case the liquid is driven through the porous tubes by the pump. Ionic liquid leakage and air bubble ingestion are resisted by the capillary bubble point within the pores of the tubes. Direct contact of the air with the liquid is maintained at each pore of the tubes. The active interface area is a linear function of the tube effective surface porosity. A gradient in pore size along the tubes may be exploited to control the pressure losses and stability.

Further details of the Fig. 4 design include 18 porous contactors of diameter 1.5 mm and varying lengths. Pore size varies along each contactor between 20 and 200 μm. The axial porous gradient of the contactors is used to balance the pressure gradient intrinsic to the pressure driven manifold design. The pore structure seeks to equalize flow within and between individual contactors. Cylindrical contactors provide full circumferential contact to the air flow. As the diameter and wall thickness of the contactors reduces the reaction density of the system increases significantly. For a system with 1.5 mm diameter contactors, a radial gap between contactors of 1.5 mm, and 2 mm air gap between layers of contactors, the reaction area per volume is 0.22; this number assumes the entire contactor surface is an active site for reaction. For comparison, the reaction density of the rectangular array corner flow design is 0.37. This design is readily expandable in the axial direction by simply stacking more 'disks'. The reactor can also be expanded in airflow cross section by grouping multiple reactive flow channels together. The porous pillars may be less susceptible to bubble ingestion and macroscopic contamination than interior corner capillary flow designs, but the porous tube approach may be susceptible to contaminants.

The basic operations of these low-g designs were demonstrated in terrestrial tests of 3D printed scaled models to be discussed next.

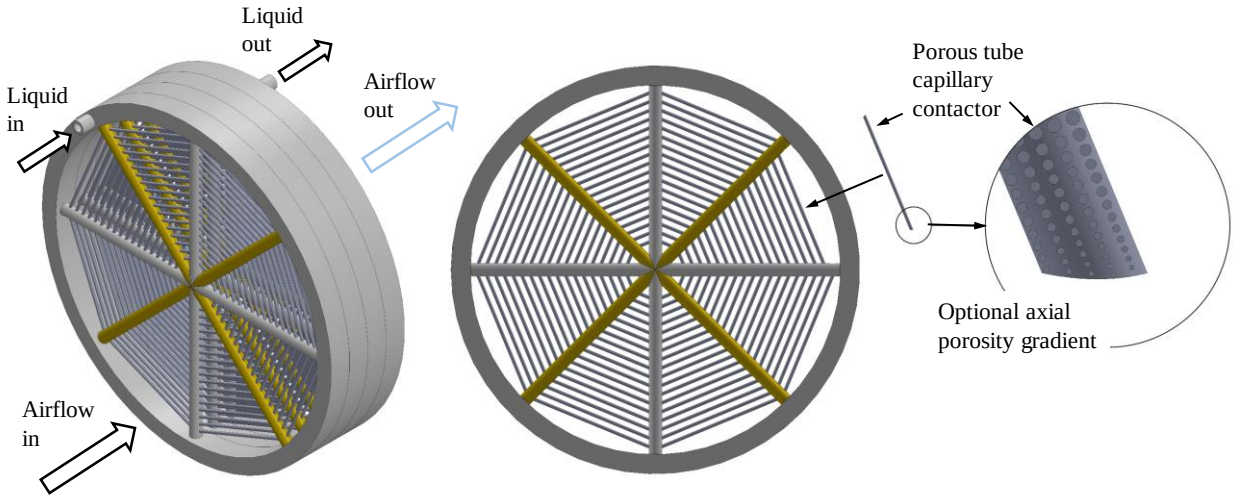

Fig. 4. Stackable 4-tier open wedge corrugated wall axial low-g contactor with sectional cutaway views illustrating planform view and direct contact porous tubes. In this design, capillary forces are used to stabilize the interfaces along the porosity gradient of the tubes, which allows for increasingly stable interfaces despite the increasing pressure drop across the tube wall. The active interface area is a linear function of the tube effective surface porosity.

Terrestrial Demonstration 3D-Printed Contactors

With regular guidance from the PI, to demonstrate the potential of complex 3D printed nested-manifold flow networks, over 15 scaled devices were designed, printed, and tested in the laboratories at Portland State University by four BSME students. Three of the designs are reported here that received the most interest, experimental attention, and practical promise. (Scaled models of these designs are solid modelled, 3D printed, and tested in the laboratory, but we note that

without direct programming, full size versions of these designs routinely crash the design software—in this case SolidWorks.)

Hollow Tube Vertical Up-flow

A solid model and 3D printed device image are presented in Fig. 5 of a hollow tube vertical up-flow contactor. For this device the liquid is forced up parallel hollow tube passageways from a single manifold. The circular opening at the top of each tube allows the liquid to form a meniscus, which then overflows uniformly over the side of the outer tube walls forming a stable thin annular fill. The film thickness may be controlled by the flow rate of the liquid from the pump. Solid models are provided in Fig. 5a and b. The image of Fig. 5c shows the device in operation. It is difficult to observe the fluid motion by eye due to the stability of the thin films. However, high flow rates are achieved by this gravity-driven direct contact approach. Up to 4 mL/s were achieved by this 72 by 54 by 32 mm device. Surface area densities are achieved with fine control of tube dimensions and spacing. A special 3D Systems ProJet 3D printer is required for such designs in order to remove the support material from a nearly fully enclosed cavity of the delivery manifold.

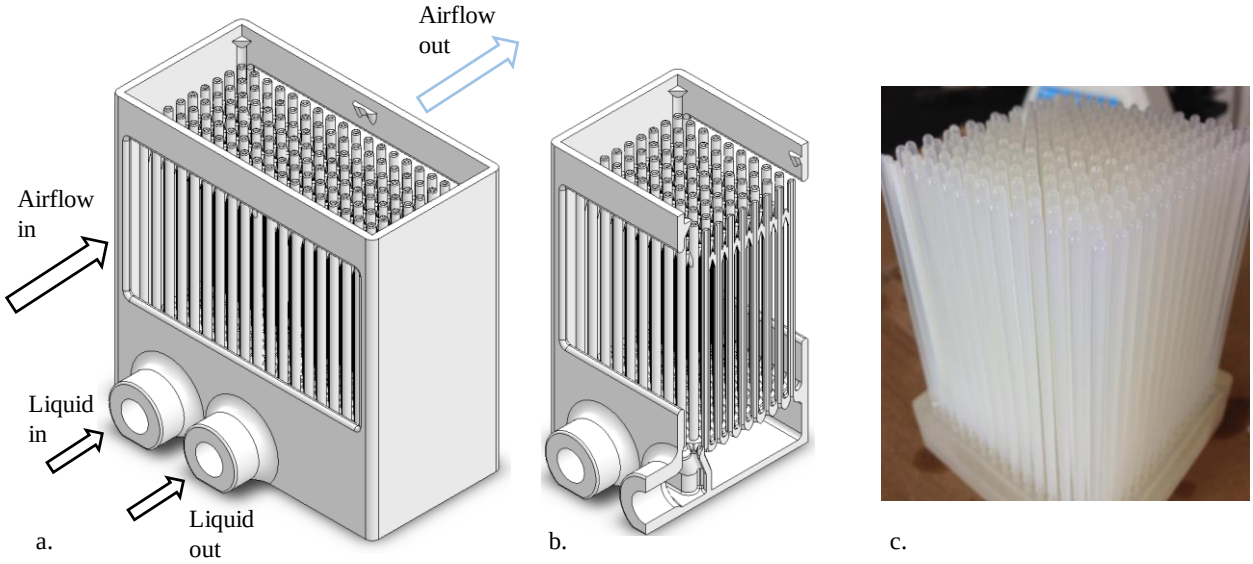

Fig. 5. 3-D printed hollow tube vertical up-flow contactor where the liquid is forced up parallel hollow tube passageways from a single manifold (reservoir). The opening at the top of each tube allows liquid to form a meniscus which uniformly pours over the side of the outer tube walls forming a stable uniform thin film. The film thickness may be controlled by the flow rate of the liquid from the pump: a. Solid model perspective highlighting fluid flow paths, b. sectional view showing fill manifold below, and c. image of the device in operation. Nearly hemispherical menisci are visible at the top of each hollow tube.

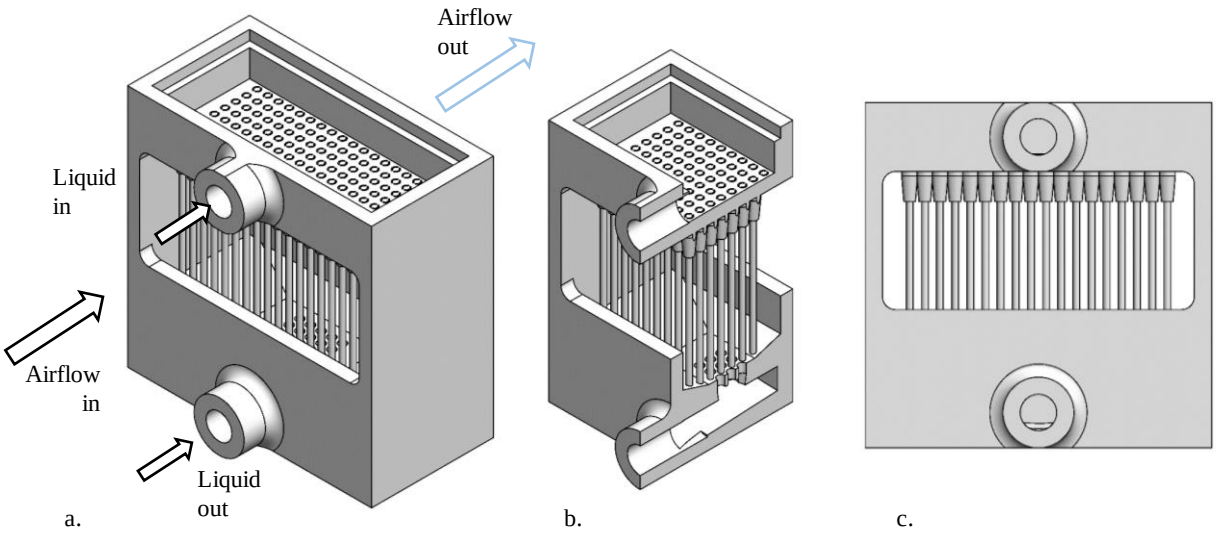

Fig. 6. Solid pin gravity driven reactor is shown. Top reservoir is filled with ionic liquid that flows through the nozzle matrix and exits creating a thin sheet of fluid around the pins. The feed nozzles have an annular gap of 0.3 mm. The distance between pins is 1.9 mm. When the annular gap is too large a capillary bridge/droplet instability develops between pillars and within the tapered geometry between the outer surface of the nozzles. These instabilities are not present for narrower annular gap of 0.2 mm was used for nozzles.

Gravity Feed Annular Film Extruder

A gravity driven annular gap pin reactor is shown in Fig. 6. Top reservoir acts as a hopper and is filled with ionic liquid that flows through annular 'nozzles' at the top of each solid cylindrical post which passes up into the hopper. The annular nozzles create a thin annular films around the post that drain uniformly downward. The feed nozzles have an annular gap of 0.3 mm. The distance between pins is 1.9 mm. When the annular gap is too large, the flow is too fast, and transient capillary bridges between posts are observed/droplet instability develops between pillars. These bridges do not harm the perfoemance of the device, but they do introduce some periodicity to the otherwise steady flow. Such 'instabilities' are not present for narrower annular gaps of 0.2 mm or less. For this device in particular, we observed manufacturing variances in the 3D prints arising from the incomplete clearing of support material which lead to local variations in flow rate distributions and wettability. Both effects lead to local non-uniformities in the flow.

Gravity-Fed Corrugated Wedge Wall

In Fig. 7 is presengted a solid model of 3D printed and tested gravity-fed corrugated wedge wall device showing liquid and air flow paths with a cutaway and front view. In the cutaway view of Fig. 7b an exploded view of the corrugated wedge wall section is shown. We note that both sides of the corrugated wall are wetted by the liquid and thus the active surface area is simply the effected wall area of the projected corrugations. High surface areas per unit volumes are possible with this

device due to the inherent stability (under-pressure) if the menisci along the wedges forming the corrugations of each wall.

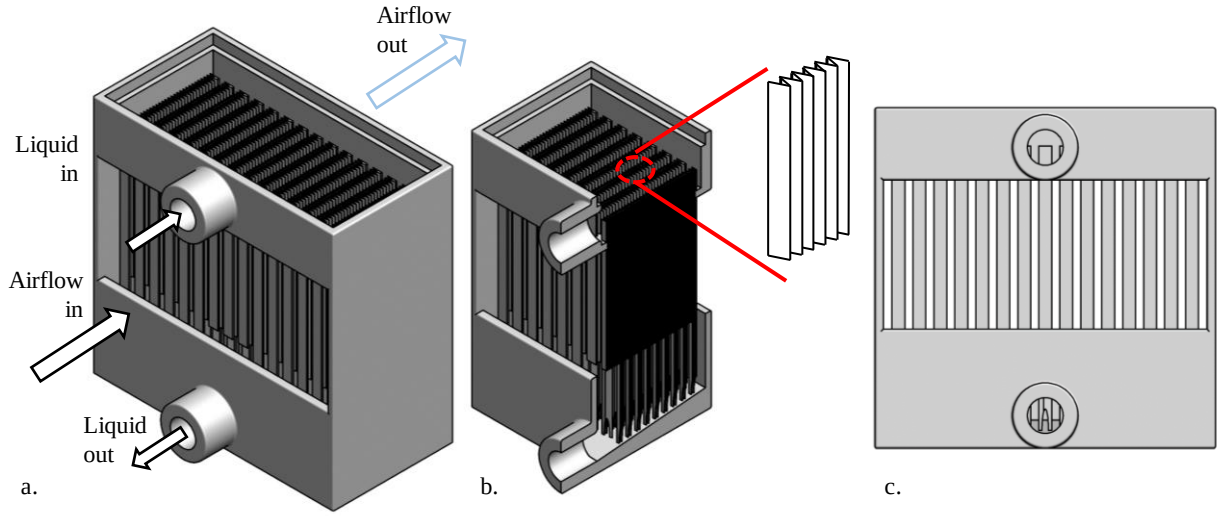

Fig. 7. a. Solid model of 3D printed gravity-fed corrugated wedge wall showing liquid and air flow paths. A cutaway view is shown in b. with exploded view of corrugated wedge wall section—note that both sides flow view of device.

The Fig. 1 design was manufactured using *Multi-Jet* printing technology from *3D Systems*. Dimensions of the test part include 885 channels of 15° wedge half-angles and 1 mm wide by 1.87 mm deep wedge cross-sections. The channels are gravity-fed by the upper reservoir and drained to a lower basin. Geometry and surface tension create a curved interface between the liquid columns and ambient air which increases surface area by as much as 70% over a planer surface of equal height. Negative capillary pressures associated with the free surface work to maintain location of the fluid inside the corner and decrease possibilities of fluid-shearing from air cross-flow. Capillary driven flow along the axial direction of the corner can act as the replacement for gravity in environments when the effects of gravity are small (low-gravity), but in this 1-g device capillary forces enhance the performance of the device by slightly speeding the flows along the corners. The features of this design are small and compact; design software limitations are again evident when printing devices en masse. Without careful removal of the print support material the inlets to each corner flow cold be clogged.